Journal of Applied Physics

Electronic structure of epitaxially grown and regrown GaN pn junctions characterized by scanning Kelvin probe and capacitance microscopy

Cite as: J. Appl. Phys. **131**, 015704 (2022); https://doi.org/10.1063/5.0071422
Submitted: 14 September 2021 • Accepted: 12 December 2021 • Published Online: 04 January 2022

Tae-Hyeon Kim, Kai Fu, Chen Yang, et al.

Journal of Applied Physics ARTICLE scitation.org/journal/jap

Electronic structure of epitaxially grown and regrown GaN pn junctions characterized by scanning Kelvin probe and capacitance microscopy

Cite as: J. Appl. Phys. **131**, 015704 (2022); doi: 10.1063/5.0071422
Submitted: 14 September 2021 · Accepted: 12 December 2021 ·
Published Online: 4 January 2022

Tae-Hyeon Kim,[1] Kai Fu,[2] Chen Yang,[2] Yuji Zhao,[2] and Edward T. Yu[1,a)]

AFFILIATIONS

[1]Microelectronics Research Center, The University of Texas at Austin, 10100 Burnet Rd., Building 160, Austin, Texas 78758, USA
[2]School of Electrical, Computer and Energy Engineering, Arizona State University, Tempe, Arizona 85287, USA

Note: This paper is part of the Special Topic on Defects in Semiconductors.
[a)]**Author to whom correspondence should be addressed:** ety@ece.utexas.edu

ABSTRACT

Epitaxial regrowth of GaN pn junctions is a key technology for realization of a variety of high-performance GaN power electronic devices. However, the regrowth process can introduce impurities and defects that degrade a device's performance. Here, we show that scanning Kelvin probe force microscopy and scanning capacitance microscopy can be used in a cross-sectional geometry to probe dopant distributions and an electronic structure in epitaxially grown GaN pn junctions. These measurements enable profiling of potential and dopant distributions across GaN pn junctions produced by uninterrupted epitaxial growth and by regrowth on an etched surface. Clear differences are observed in comparisons to the electronic structure of these two types of junctions that can be correlated with results of complementary characterization of dopant distributions reported for similarly grown structures. These measurements also suggest the presence of defects in etch-and-regrow pn junction structures that extend nearly 1 μm below the regrown interface.

I. INTRODUCTION

Gallium nitride (GaN) shows outstanding promise for application in next-generation power electronics due to its high breakdown electric field, chemical stability, and robustness to high operating temperature.[1–4] However, high-performance GaN power electronic devices must overcome a variety of challenges including selective-area doping for certain high-performance device geometries[5,6] and suppression of electronically active defect formation.[7–9] A promising approach for selective-area doping as required in, for example, lateral pn junctions is etching followed by epitaxial regrowth.[10] However, interfaces formed using this approach tend to have higher leakage current due to defects induced by the dry etching process.[11] Characterization of such defects, including local inhomogeneities associated with the spatial distribution of defects, often requires that measurements be performed on cross-sectional surfaces exposed by cleaving or etching.[12,13] Scanning probe microscopy performed in a cross-sectional geometry offers unique capabilities for the characterization of the electronic structure with nanoscale spatial resolution in both the vertical and lateral directions in epitaxial layers and devices.[14–21]

In this article, we present cross-sectional scanning Kelvin probe force microscopy (SKPM) and scanning capacitance microscopy (SCM) measurements performed on epitaxially as-grown and etch-then-regrow GaN pn junctions. Cross-sectional SKPM and SCM are shown to enable profiling of potential and dopant distributions in GaN pn junctions and also detection of variations in local dopant concentration, particularly at low to moderate doping levels. These studies reveal clear differences in the electronic structure of these two types of junctions that can be correlated with results of complementary characterization of dopant distributions

reported for similarly grown structures and suggest the presence of defects in etch-then-regrow pn junction structures extending nearly 1 μm below the regrown interface.[22]

II. EXPERIMENT

All samples for these studies were grown by metalorganic chemical vapor deposition (MOCVD) on *c*-plane *n*-type GaN substrates with a carrier concentration of $\sim 10^{18}$ cm^{-3}. 6500 nm of unintentionally doped (UID) GaN was grown initially for all samples. For the as-grown pn junction structures, as shown in Fig. 1(a), 400 nm of p-type GaN was grown directly on the UID GaN layer without any growth interruption, using Cp_2Mg as the dopant source. For the etched + regrown structure shown in Fig. 1(b), the UID GaN layer was removed from the growth chamber and etched using an inductively coupled plasma (ICP) etch system with 400 W of ICP etching power to remove approximately 1500 nm of GaN. A 400 nm p-type GaN layer was then grown atop the etched surface

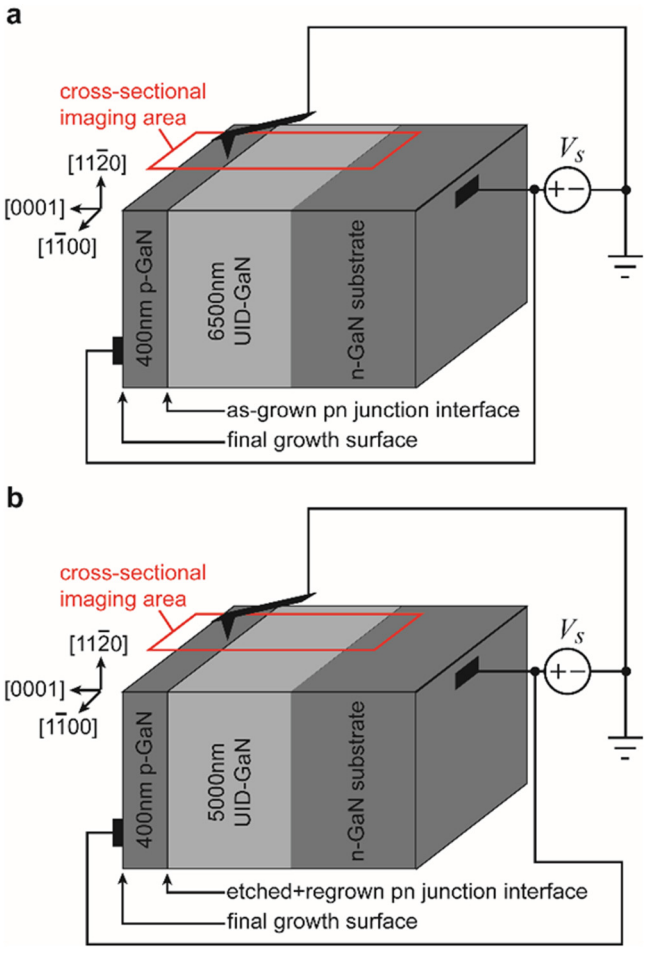

FIG. 1. Schematic illustrations of cross-sectional SKPM and SCM characterization of (a) as-grown and (b) etch-and-regrow GaN pn junctions. Bias voltages V_s are applied to the sample with the probe tip grounded.

under the same conditions as for the as-grown pn junction structure. All samples then underwent a rapid thermal anneal at 700 °C for 20 min in N_2 ambient to activate the p-type dopants.

Cross-sectional surfaces were prepared by polishing chips approximately 3×5 mm^2 in area from their original thickness of 300 μm to a final thickness of 200 μm. 800-grit SiC abrasive was used on a polishing plate rotating at 300 rpm to thin samples via polishing on the back side of the GaN substrate. The polishing rate was 10 μm/min. Polished samples were then cleaved along a [1$\bar{1}$00] direction to expose a (11$\bar{2}$0) cross-sectional surface. Cleaved samples were then mounted in a custom-built sample holder for scanned probe microscopy (SPM) measurements. Typical cleaved surfaces used for SPM measurements exhibited root-mean-square (RMS) surface roughness of $\sim$2 nm over an area of 5×5 μm^2. Such low roughness is required to minimize the effect of surface topography on cross-sectional SKPM and SCM measurements.[23] All SPM measurements were performed using a Bruker Dimension Icon scanned probe microscope system. Both SKPM and SCM measurements were performed using Bruker MESP-RC-V2 Co-Cr conductive probe tips, which have a typical tip radius of 35–50 nm. In all cases, bias voltages were applied to the sample relative to a grounded probe tip, with the electrical contact made at both the top (p-GaN epitaxial layer) and bottom (n-GaN substrate) of the sample. All measurements were performed at room temperature in ambient air conditions, without any ambient room illumination.

SKPM measurements[24–26] were performed with a tip lift height of 30 nm and an ac tip drive voltage of 500 mV. In brief, SKPM yields a measurement of the difference in local surface potential between the conductive AFM probe tip and the sample surface below the tip apex. The quantities plotted as "Potential" in subsequent figures correspond to the sample bias voltage V_s that must be applied to the probe tip to offset the work function difference between the probe tip and the sample surface. Because the work function of p-type GaN is greater than that of n-type GaN, this applied potential is more positive for p-type GaN than for n-type GaN.

SCM measurements were performed in contact mode as a function of dc voltage applied to the sample, with an ac sample voltage amplitude of 1.5 V at 90 kHz. The measured SCM signal corresponds to the derivative of the high-frequency tip-sample capacitance with respect to the sample voltage V_s, averaged over the range of ac voltage modulation. In this article, we present the SCM data signal, which consists of the dC/dV amplitude signal with a sign corresponding to that of dC/dV. The sign of the SCM data signal indicates the type of carrier being modulated; a low-signal amplitude indicates high carrier concentration while a high signal amplitude indicates low carrier concentration.[23] Also, the SCM signal is small when the sample is in accumulation or at its maximum depletion depth below the surface and nonzero for voltages between these regimes of behavior. For voltages applied to the sample with the probe tip grounded, as shown in Fig. 1, a positive SCM signal is measured for p-type GaN and a negative signal for n-type GaN.

III. RESULT AND DISCUSSION

Figure 2(a) shows an AFM topograph and a simultaneously acquired SKPM image of a 3000×500 nm^2 area of the cleaved

cross-sectional surface near the final growth surface of an as-grown GaN pn junction, as illustrated schematically in Fig. 1(a). Figure 2(b) shows line profiles extracted from each image in the [0001] direction, averaged across the 500 nm extent of each image in the [1$\bar{1}$00] direction. The position of the final growth surface is easily determined from the topographic image, and the position of the as-grown pn junction interface is taken to be 400 nm from the final growth surface. A series of small steps, 10–20 nm in height, is visible within the p-GaN layer, but these appear to have only a slight effect on the measured surface potential shown in Fig. 2(b).

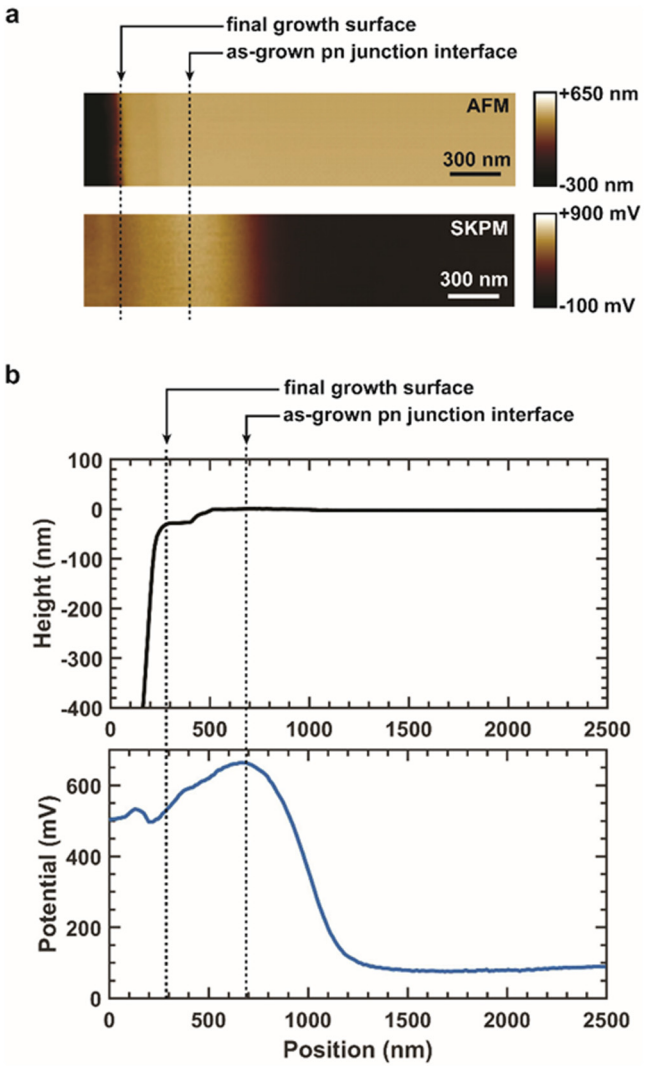

FIG. 2. (a) AFM topograph (top) and SKPM image (bottom) of the as-grown pn junction structure and (b) line profiles of topography and surface potential difference extracted from the images shown in (a). The line profiles are constructed by averaging each signal in the vertical image direction across the entirety of each image shown in (a).

From the SKPM surface potential difference line profile in Fig. 2(b), we see that the work function of the cross-sectional surface reaches a maximum value very close to the position of the as-grown pn junction interface. The work function then decreases gradually across the junction depletion region, which we estimate from the surface potential profile to be ∼650 nm in width. The measured shift in the surface potential across the depletion layer is 590 mV, which is considerably less than the expected potential shift of approximately 3.3 V that would be expected for the dopant concentrations present in the junction. We attribute this difference to partial pinning of the Fermi level at the cross-sectional surface, which can arise from the presence of surface states on the cleaved surface.[27,28] The likely presence of such partial pinning on the cross-sectional surface combined with the complex three-dimensional geometry of the tip and pn junction also makes it difficult to interpret the detailed shape of the potential profile directly in terms of ionized dopant charge densities in the pn junction depletion layer. However, we expect the total measured junction depletion layer width to be relatively insensitive to such effects. Assuming then that the p-type dopant concentration N_a is much greater than the n-type dopant concentration N_d in the vicinity of the pn junction, we can easily show that[29]

$$N_d \approx \frac{2\varepsilon_s V_{bi}}{qW^2},$$

where ε_s is the dielectric constant of GaN, V_{bi} is the built-in potential of the pn junction, q is the magnitude of the electron charge, and W is the junction depletion layer width. Taking $\varepsilon_s = 8.9\varepsilon_0$ where $\varepsilon_0 = 8.85 \times 10^{-12}\,F/m$, $q = 1.602 \times 10^{-19}$ C, $V_{bi} = 3.3$ V, and $W = 650$ nm, we obtain $N_d = 7.7 \times 10^{15}\,\mathrm{cm}^{-3}$, which is comparable to the typical donor concentration of $\sim 10^{16}\,\mathrm{cm}^{-3}$ in UID GaN.[23,30] We also see in Fig. 2(b) that the measured surface potential decreases slightly in the [0001] direction, i.e., moving toward the final growth surface, within the p-type GaN region. This may occur due to the existence of a slightly different Fermi level pinning position on the as-grown (0001) surface compared to that on the cleaved (11$\bar{2}$0) cross-sectional surface, or to reduction of the total tip-sample capacitance very close to the sample edge at the final growth surface. Neither of these possibilities is expected to influence the characterization of the electronic structure at or below the as-grown or etched + regrown interfaces of interest in this study.

Figure 3(a) shows the surface potential difference profiles extracted from SKPM imaging of both as-grown and etched + regrown pn junction structures, as shown in Figs. 1(a) and 1(b), respectively, with the locations of the final growth surfaces as determined from topographic images aligned in the plot. While the surface potential differences measured for both structures are nearly the same at the final growth surface, they diverge within the p-GaN region below the surface, and at the pn junction interface, the surface potential difference is significantly lower in the etched + regrown structure than in the as-grown structure. Prior studies on identically grown structures[22] and a variety of other GaN junction structures produced by etching followed by epitaxial regrowth[11,31] have indicated that there is typically a very high concentration, ranging from 10^{18} to $10^{19}\,\mathrm{cm}^{-3}$, of Si present at the regrown interface. The reduced surface potential difference observed at the

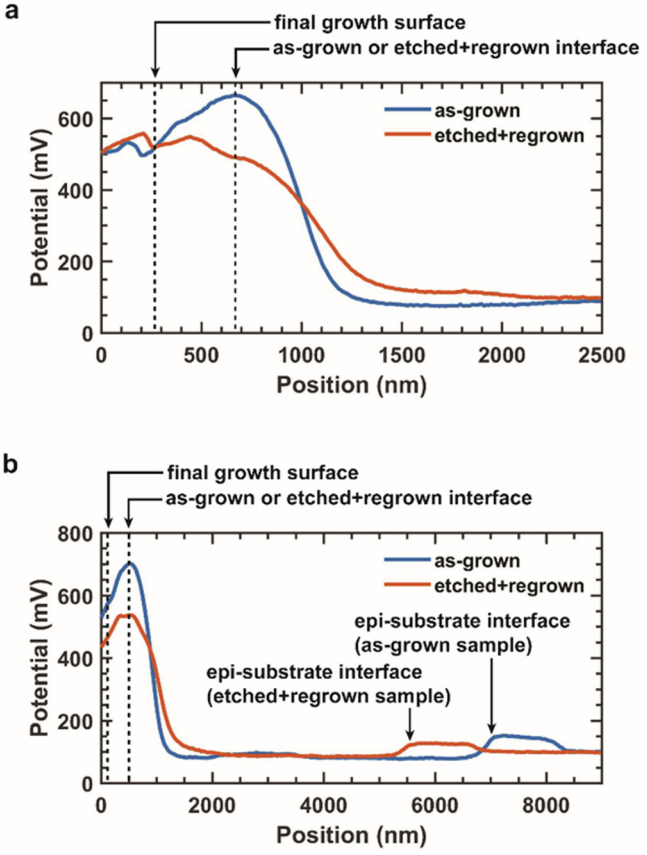

FIG. 3. Line profiles of both as-grown and etched + regrown pn junction structures showing (a) the region in the immediate vicinity of each pn junction and (b) the entire epitaxial layer structure and top portion of the n-GaN substrate. The locations of the final growth surface, the pn junction interface, and the epitaxial layer–substrate interface are indicated.

etched + regrown pn junction interface in Fig. 3(a) is consistent with the presence at the interface of a high concentration of Si, which would partially or completely compensate the p-type dopants and lead to a reduction in work function and surface potential difference measured at the interface. The actual reduction in surface potential may be underestimated in these measurements due to averaging of the tip-sample electrostatic interaction over the finite tip size and due to the 30 nm lift height employed in the SKPM measurement.

Also evident in Fig. 3(a) is an increase in the depletion layer width in the etched + regrown junction compared to that in the as-grown junction. We estimate from Fig. 3(a) that the pn junction depletion layer width for the etched + regrown junction is approximately 950 nm compared to 650 nm for the as-grown junction. This observation is consistent with the creation of defects below the regrown interface by the dry etching process that partially compensates, e.g., by carrier trapping, the charge associated with ionized dopants introduced into the pn junction depletion layer during the epitaxial growth process. In addition, based on the measured depletion layer width, these defects appear to influence the junction structure to depths approaching a micrometer below the etched + regrown interface.

Figure 3(b) shows surface potential difference profiles extracted from the SKPM image of $10 \times 10\,\mu m^2$. SKPM images extend from the final epitaxial growth surface to the n-type GaN substrate region, averaged over a 2000 nm extent of each image in the $[1\bar{1}00]$ direction. A number of features are evident in the profiles. First, both the as-grown and etched + regrown structures exhibit a layer of increased surface potential difference just below the substrate–epitaxial layer interface. This feature is most likely a consequence of defects or impurities present near the surface of the substrate prior to epitaxial growth; such defects could trap electrons, leading to an increase in work function and in the corresponding measured surface potential difference. This behavior is, as expected, unaffected by the differences in growth and etching procedures associated with the pn junction interface, which is several micrometers above the substrate–epitaxial layer interface, but helps validate the ability of cross-sectional SKPM surface potential difference profiles to reveal variations in the electronic structure within an epitaxial layer or a substrate. Figure 3(b) also reveals smaller variations in measured surface potential difference within the UID layer in the as-grown junction structure. We attribute these, based on SCM measurements shown in Fig. 4, to small variations in donor concentration with depth.

Scanning capacitance microscopy (SCM) and scanning capacitance spectroscopy (SCS) measurements provide additional insights into the electronic structure of as-grown and etched + regrown pn junction structures. Figure 4 shows a series of SCM images of the as-grown pn junction structure in the geometry shown in Fig. 1(a), obtained at dc bias voltages ranging from −6 to +4 V. The locations of the final growth surface, the as-grown pn junction interface, and the substrate–epitaxial layer interface are indicated for each image. The clear contrast in the SCM images, corresponding to changes in dopant concentration or other aspects of the electronic structure introduced during epitaxial growth, are evident. Smaller variations are occasionally observed, particularly in the UID GaN region, along the $[1\bar{1}00]$ direction, i.e., parallel to the pn junction interface. A detailed examination of the dependence of SCM signal values on dc bias voltage provides insight into the electronic properties of the structure at different locations and their correlation with results of SKPM potential profiles as shown in Fig. 3.

Figure 5 shows a series of scanning capacitance spectra extracted from $15 \times 15\,\mu m^2$ bias-dependent SCM images of the as-grown pn junction structure such as those shown in Fig. 4. The spectra shown in Fig. 5(b) were extracted at the locations indicated in Fig. 5(a), with each point plotted corresponding to the SCM signal measured at the indicated dc sample bias voltage and position in the [1000] direction, averaged across a 3000 nm distance in the lateral $[1\bar{1}00]$ direction located at the bottom of each image. At location 1, within the p-type GaN layer, the dependence of the SCM signal on dc bias voltage is as expected for p-type GaN: the SCM signal, which is proportional to dC/dV, the derivative of the capacitance with respect to the applied bias voltage, is very small at very positive or very negative dc bias voltages for which the tip-sample capacitance is in accumulation or high-frequency

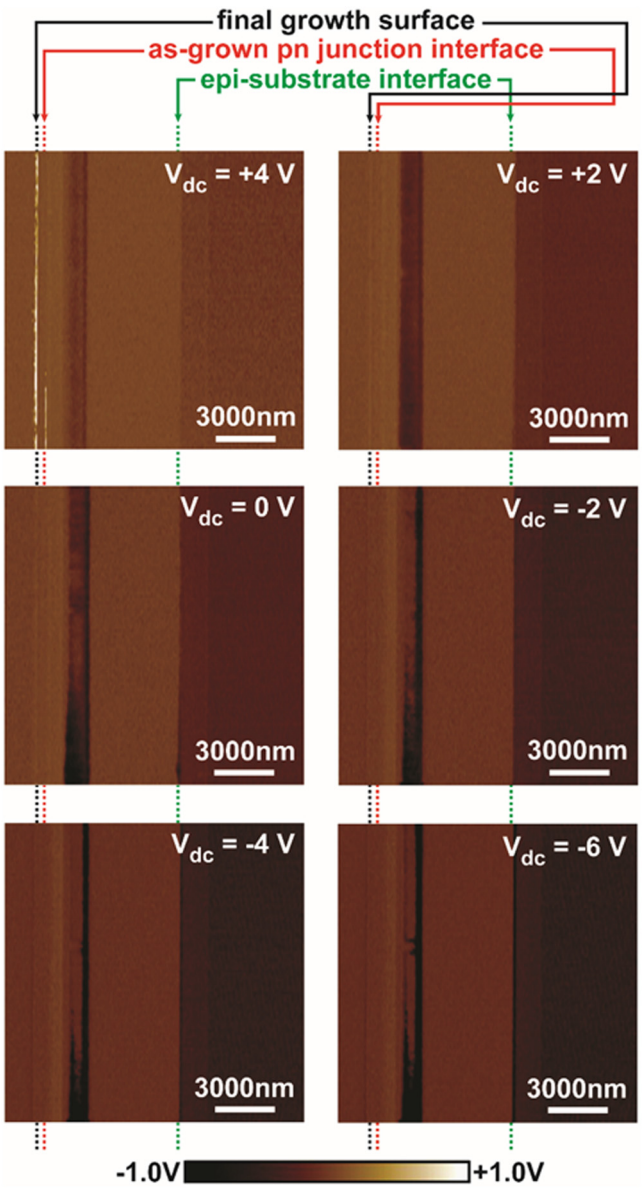

FIG. 4. $15 \times 15\,\mu m^2$ SCM images of the as-grown GaN pn junction structure in the geometry shown in Fig. 1(a) for dc bias voltages of +4, +2, 0, −2, −4, and −6 V. Positions of the final growth surface, the pn junction interface, and the epitaxial layer–substrate interface are indicated for each image.

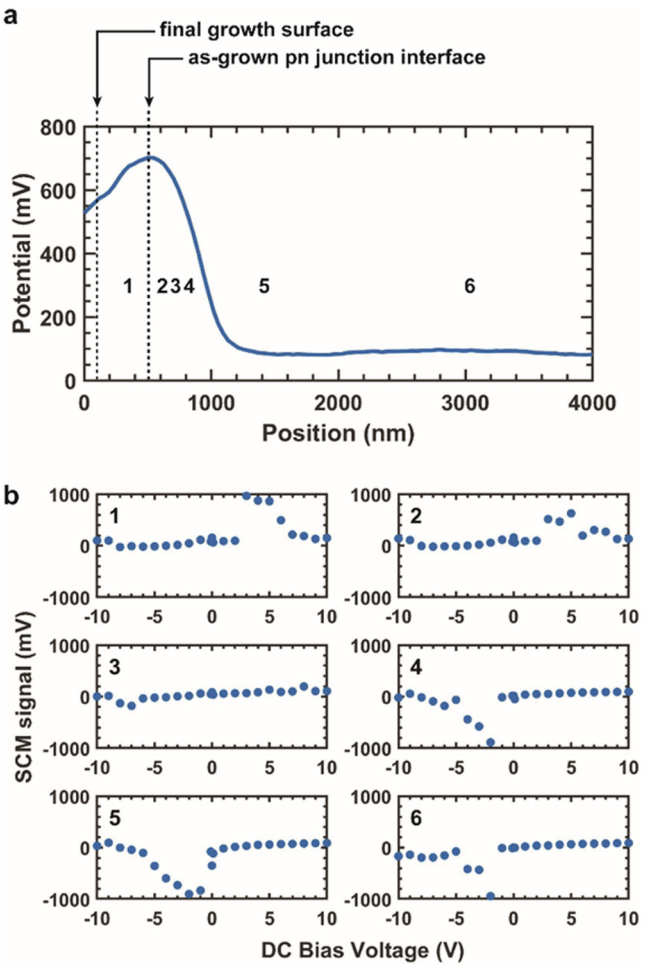

FIG. 5. (a) Line profile of the surface potential difference measured by SKPM for as-grown pn junction structure in geometry shown in Fig. 1(a). The positions of the final growth surface and the pn junction interface are indicated. (b) SCM signal spectra at locations 1–6 indicated in (a), extracted from SCM images of the as-grown pn junction at bias voltages ranging from −10 to +10 V in 1 V steps. The distances of each location below the final growth surface are approximately 240, 530, 650, 710, 1310, and 2950 nm for locations 1, 2, 3, 4, 5, and 6, respectively.

depletion, respectively, and a positive SCM signal is measured as the dc bias voltage sweeps the tip-sample capacitance through depletion between these regimes. Similar behavior, but with a smaller SCM signal amplitude, is observed at location 2, near the p-type edge of the pn junction depletion layer. The reduction in SCM signal amplitude can be explained as a consequence of the very low hole concentration within the junction depletion layer combined with some spillover of holes from the adjacent p-type region. At location 3, well within the pn junction depletion region, the SCM signal at all bias voltages is very low due to the absence of mobile carriers in the pn junction depletion region, leading to small tip-sample capacitance and therefore dC/dV at all dc bias voltages.[23]

At location 4, within the pn junction depletion region but closer to the n-type GaN layer, the SCM signal spectrum begins to resemble that of n-type GaN: the SCM signal is very small at large positive or negative bias voltages and becomes negative at intermediate bias voltages as the dc bias voltage sweeps the tip-sample capacitance from accumulation (at negative sample bias voltages) to high-frequency depletion (at positive bias voltages). This

behavior can occur even within the pn junction depletion region due to spillover of electrons from the adjacent n-type GaN layer, once the distance to the n-GaN layer is sufficiently small. At location 5, within the UID GaN layer, the dependence of the SCM signal on dc bias voltage is again as expected for n-type GaN. Finally, at location 6, n-type SCM signal contrast is observed but the SCM signal amplitude is reduced compared to that at location 5. Similar behavior has been reported for lightly doped n-type GaN[20] and attributed to the fact that at sufficiently low donor concentrations in GaN, too few electrons are available in the vicinity of the probe tip to enable full formation of an electron accumulation layer below the probe tip apex. The SCM signal spectrum at location 6, therefore, suggests that the donor concentration at that location is lower than that of the surrounding material. The increased SKPM potential signal measured at that location, as shown in Fig. 5(a), is consistent with this interpretation.

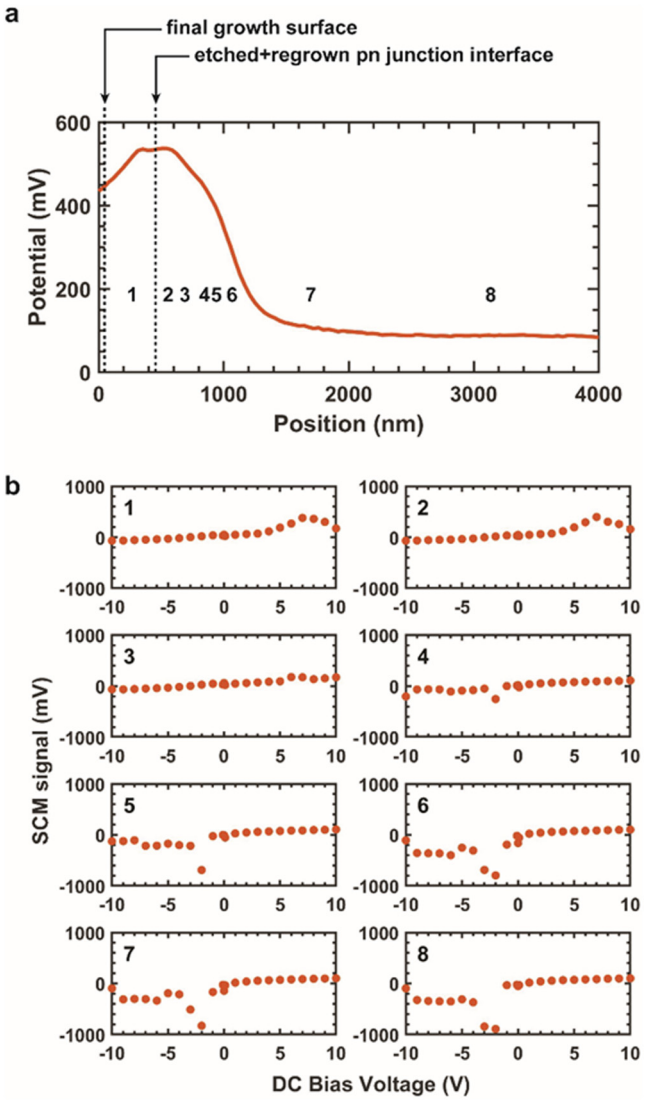

FIG. 6. (a) Line profile of surface potential difference measured by SKPM for the etched + regrown pn junction structure in geometry shown in Fig. 1(b). The positions of the final growth surface and the pn junction interface are indicated. (b) SCM signal spectra at locations 1–8 indicated in (a), extracted from SCM images of the etched + grown pn junction at bias voltages ranging from −10 to +10 V in 1 V steps. The distances of each location below the final growth surface are approximately 240, 530, 650, 830, 940, 1000, 1650, and 3070 nm for locations 1, 2, 3, 4, 5, 6, 7, and 8, respectively.

Figure 6 shows a series of scanning capacitance spectra extracted from SCM images of the etched + regrown structure shown in Fig. 1(b). The spectra shown in Fig. 6(b) were extracted at the locations indicated in Fig. 6(a) and averaged in the lateral direction in the same manner as the SCM spectra shown in Fig. 5. At location 1, within the p-type GaN layer, the SCM signal behaves as expected for p-type GaN. The signal amplitude at this location is lower than that for the as-grown pn junction structure, shown in Fig. 5(b), most likely due to variations in the SCM signal amplitude that can occur as a result of differences in tip geometry, particularly the tip radius near its apex.[32] At location 2, within the pn junction depletion region but close to the adjacent p-type GaN layer, the SCM signal spectrum exhibits behavior characteristic of p-type GaN due to the spillover of holes from the adjacent p-type GaN that enables the formation of a hole accumulation layer at the location for sufficiently large positive sample bias voltages. At location 3, farther within the pn junction depletion region, the SCM signal at all bias voltages is very low due to the absence of mobile carriers, as was observed within the depletion region of the as-grown junction. In the case of the etched + regrown junction, however, the reduced signal amplitude persists over a larger region, as indicated by SCM signal spectra for locations 4 and 5. Non-negligible SCM signals are observed in these locations only at −2 V, with very small SCM signals measured at all other bias voltages. At location 6, within the pn junction depletion region but closer to the n-type GaN layer, the SCM signal spectrum begins to appear like that of n-type GaN, behavior similar to that observed at the corresponding location in the as-grown pn junction structure. At locations 7 and 8, within the UID GaN layer, behavior corresponding to n-type GaN is observed, as expected. These results confirm the presence of a substantially larger depletion region in the etched + regrown pn junction structure relative to that in the as-grown junction, corroborating the conclusion drawn from the SKPM measurements. For both junction structures, spillover of electrons into the pn junction depletion region from the adjacent n-type GaN layer can extend up to ∼400 nm into the junction depletion region, while spillover of holes extends less than 200 nm into the junction depletion region.

IV. CONCLUSION

In summary, we have used cross-sectional SKPM and SCM to characterize the electronic structure of MOCVD-grown GaN pn junctions produced either by uninterrupted epitaxial growth or by dry etching of a UID GaN epitaxial layer followed by epitaxial regrowth of p-type GaN on the etched surface. Cleaving to expose a $(11\bar{2}0)$ cross-sectional surface for scanned probe imaging allows the electronic structure of such junctions to be probed directly with nanoscale spatial resolution. Cross-sectional SKPM imaging is

shown, for the first time, to enable profiling of potential distributions in both types of GaN pn junctions and also detection of variations in local dopant concentration, particularly at low to moderate doping levels, due to corresponding shifts in local surface potential. Cross-sectional SCM measurements corroborate the dopant distributions deduced from SKPM measurements and also show that tip-induced spillover of mobile carriers near pn junction depletion layer edges can significantly influence SCM measurements. Comparisons of cross-sectional SKPM and SCM measurements for as-grown and etched + regrown GaN pn junctions reveal clear differences in the electronic structure at and near the pn junction interfaces. SKPM characterization reveals a local reduction in surface potential at the etched + regrown interface consistent with widely reported observations of Si dopant spikes that can be present at such interfaces, while both SKPM and SCM measurements indicate that etched + regrown junctions exhibit an increased pn junction depletion layer width most likely associated with etch-induced defects that extend nearly a micrometer below the etched + regrown interface.

ACKNOWLEDGMENTS

This work was supported primarily by the ARPA-E PNDIODES program monitored by Dr. Isik Kizilyalli (Grant No. DE-AR0000868) and performed in part at the University of Texas Microelectronics Research Center, a member of the National Nanotechnology Coordinated Infrastructure (NNCI), which is supported by the National Science Foundation (NSF) (Grant No. ECCS-2025227). We thank Jae Hyun Kim for instruction regarding compound semiconductor polishing processes.

AUTHOR DECLARATIONS

Conflict of Interest

The authors have no conflicts to disclose.

DATA AVAILABILITY

The data that support the findings of this study are available within the article.

REFERENCES

[1]H. Xing, S. Keller, Y.-F. Wu, L. McCarthy, I. P. Smorchkova, D. Buttari, R. Coffie, D. S. Green, G. Parish, and S. Heikman, J. Phys. Condens. Matter **13**, 7139–7157 (2001).
[2]S. Chowdhury, B. L. Swenson, M. H. Wong, and U. K. Mishra, Semicond. Sci. Technol. **28**, 074014 (2013).
[3]N. R. Glavin, K. D. Chabak, E. R. Heller, E. A. Moore, T. A. Prusnick, B. Maruyama, D. E. Walker, Jr., D. L. Dorsey, Q. Paduano, and M. Snure, Adv. Mater. **29**, 1701838 (2017).
[4]Y. Zhang, A. Dadgar, and T. Palacios, J. Phys. D: Appl. Phys. **51**, 273001 (2018).
[5]B. J. Baliga, *Fundamentals of Power Semiconductor Devices* (Springer-Verlag, 2008).
[6]W. Sung, E. V. Brunt, B. J. Baliga, and A. Q. Huang, IEEE Electron Device Lett. **32**, 880–882 (2011).
[7]G. Koblmüller, R. M. Chu, A. Raman, U. K. Mishra, and J. S. Speck, J. Appl. Phys. **107**, 043527 (2010).
[8]H. Xing, S. P. DenBaars, and U. K. Mishra, J. Appl. Phys. **97**, 113703 (2005).
[9]A. Agarwal, O. Koksaldi, C. Gupta, S. Keller, and U. K. Mishra, Appl. Phys. Lett. **111**, 233507 (2017).
[10]M. Monavarian, G. Pickrell, A. A. Aragon, I. Stricklin, M. H. Crawford, A. A. Allerman, K. C. Celio, F. Léonard, A. A. Talin, A. M. Armstrong, and D. Feezell, IEEE Electron Device Lett. **40**, 387–390 (2019).
[11]K. Fu, H. Fu, H. Liu, S. R. Alugubelli, T.-H. Yang, X. Huang, H. Chen, I. Baranowski, J. Montes, F. A. Ponce, and Y. Zhao, Appl. Phys. Lett. **113**, 233502 (2018).
[12]P. A. Rosenthal, Y. Taur, and E. T. Yu, Appl. Phys. Lett. **81**, 3993–3995 (2002).
[13]K. W. Park, E. M. Krivoy, H. P. Nair, S. R. Bank, and E. T. Yu, Nanotechnology **26**, 265701 (2015).
[14]E. T. Yu, K. Barmak, P. Ronsheim, M. B. Johnson, P. McFarland, and J.-M. Halbout, J. Appl. Phys. **79**, 2115–2121 (1996).
[15]E. T. Yu, Chem. Rev. **97**, 1017–1044 (1997).
[16]P. A. Rosenthal and E. T. Yu, J. Appl. Phys. **87**, 1937–1942 (2000).
[17]M. Sugimoto, M. Kanechika, T. Uesugi, and T. Kachi, Phys. Status Solidi C **8**, 2512–2514 (2011).
[18]V. V. Strelchuk, A. S. Nikolenko, P. M. Lytvyn, A. S. Romanyuk, Y. I. Mazur, M. E. Ware, E. A. Decuir, Jr., G. J. Salamo, and A. E. Belyaev, Phys. Status Solidi C **11**, 269–273 (2014).
[19]A. Minj, A. Cros, T. Auzelle, J. Pernot, and B. Daudin, Nanotechnology **27**, 385202 (2016).
[20]T. Zhu and R. A. Oliver, Phys. Chem. Chem. Phys. **14**, 9558–9573 (2012).
[21]M. Lamhamdi, F. Cayrel, E. Frayssinet, A. E. Bazin, A. Yvon, E. Collard, Y. Cordier, and D. Alquier, Nucl. Inst. Meth. Phys. Res. Sect. B **372**, 67–71 (2016).
[22]K. Fu, H. Fu, X. Deng, P. Su, H. Liu, K. Hatch, C. Cheng, D. Messina, R. V. Meidanshahi, P. Peri, C. Yang, T. Yang, J. Montes, J. Zhou, X. Qi, S. M. Goodnick, F. A. Ponce, D. J. Smith, R. Nemanich, and Y. Zhao, Appl. Phys. Lett. **118**, 222104 (2021).
[23]J. Sumner, R. A. Oliver, M. J. Kappers, and C. J. Humphreys, J. Appl. Phys. **106**, 104503 (2009).
[24]M. Nonnenmacher, M. P. O'Boyle, and H. K. Wickramasinghe, Appl. Phys. Lett. **58**, 2921–2923 (1991).
[25]E. T. Yu, Mater. Sci. Eng. R: Rep. **17**, 147–206 (1996).
[26]W. Melitz, J. Shen, A. C. Kummel, and S. Lee, Surf. Sci. Rep. **66**, 1–27 (2011).
[27]P. A. Alekseev, M. S. Dunaevskiy, G. E. Cirlin, R. R. Reznik, A. N. Smirnov, D. A. Kirilenko, V. Y. Davydov, and V. L. Berkovits, Nanotechnology **29**, 314003 (2018).
[28]H. R. Moutinho, R. G. Dhere, C.-S. Jiang, Y. Yan, D. S. Albin, and M. M. Al-Jassim, J. Appl. Phys. **108**, 074503 (2010).
[29]S. M. Sze and K. K. Ng, *Physics of Semiconductor Devices*, 3rd ed. (John Wiley & Sons, Inc., 2007).
[30]P. Peri, K. Fu, H. Fu, Y. Zhao, and D. J. Smith, J. Electron. Mater. **50**, 2637–2642 (2021).
[31]Y. Cordier, M. Azize, N. Baron, S. Chenot, O. Tottereau, and J. Massies, J. Cryst. Growth **309**, 1–7 (2007).
[32]D. M. Schaadt and E. T. Yu, J. Vac. Sci. Technol. B **20**, 1671–1676 (2002).